



Formalism for the **CASSIS**¹ software

Charlotte VASTEL²

Last update: August 7, 2025

First version: June 2006

¹<https://cassis.irap.omp.eu/>

²cvastel@irap.omp.eu

Contents

1	Radiative and collisional excitation of molecules	3
1.1	Radiative transfer	3
1.1.1	Population levels	3
1.1.2	Radiative transfer equation	6
1.2	Molecular column densities	10
1.2.1	Opacity	10
1.2.2	LTE Rotational diagram analysis	14
1.2.3	Non-LTE formalism	17
1.3	Abundances	20
1.3.1	H ₂ column density from CO observations	20
1.3.2	H ₂ column density from dust measurements	21
1.3.3	Comparison with chemical models	23
2	Use of a non-LTE radiative transfer code within CASSIS	25
2.1	RADEX	25
2.2	The collision database	26
3	Molecules (using the JPL or CDMS catalogs) in CASSIS	29
3.1	The Einstein A_{ul} coefficients	29
3.2	Spin symmetry separation	29

Chapter 1

Radiative and collisional excitation of molecules

The observations of molecular spectral lines are crucial to determine the physical and chemical conditions of the observed object. Nowadays, the technological advances offer a high spatial and spectral resolution and sensitivity, with a new spectral window for millimeter and submillimeter observations where most molecules emit their rotational transitions. Hundreds of transitions are now being accessible for some species and we sometimes need detailed radiative transfer modelling code to characterise the physical and chemical conditions of the object, sometimes with some background and foreground contamination. We will present in the following the basics for understanding the radiative transfer modelling (Sec. 1.1), in order to compute the column densities of the observed species (Sec. 1.2) and their chemical abundances (Sec. 1.3).

1.1 Radiative transfer

1.1.1 Population levels

When considering a multi energy level system of a considered species, we first need to evaluate the rate of transitions populating a given energy level. Figure 1.1 shows the example of a 2-level system with an upper level energy E_u and a lower level energy E_ℓ . The A_{ul} , B_{ul} and $B_{\ell u}$ parameters represent the so-called Einstein coefficients, respectively describing the spontaneous radiative de-excitation, the stimulated radiative de-excitation and the radiative excitation. The C_{ul} and $C_{\ell u}$ parameters represent the collisional de-excitation and excitation respectively (non radiative processes as they are independent of the photon interaction with the 2-level system). These rates are the collision rates per second per molecule of the species of interest and they depend on the density of the collision partner. They can be expressed as:

$$C_{ij} = \gamma_{ij} \times n_{collider} , \quad (1.1)$$

where $n_{collider}$ is the density of the collision partner which can be H_2 , Helium, electrons, depending on the properties of the observed ISM and participates to the level population.

The collisional rate coefficients γ_{ij} (in $\text{cm}^3 \text{s}^{-1}$) are the velocity-integrated collisional cross sections, and depend on the kinetic temperature (T_k) through the relative velocity of the colliding molecules and possibly also through the collisional cross sections directly. The downward collisional rate coefficients are tabulated in various databases such as LAMDA¹ and Basecol². They represent the Maxwellian average of the collisional cross section (σ), depending on the collision energy (E), the kinetic temperature (T_k) and the reduced mass (μ) of the system:

$$\gamma_{ul} = \sqrt{\frac{8kT_k}{\pi\mu}} \left(\frac{1}{kT_k}\right)^2 \int \sigma_{ul} E \exp\left(\frac{-E}{kT_k}\right) dE, \quad (1.2)$$

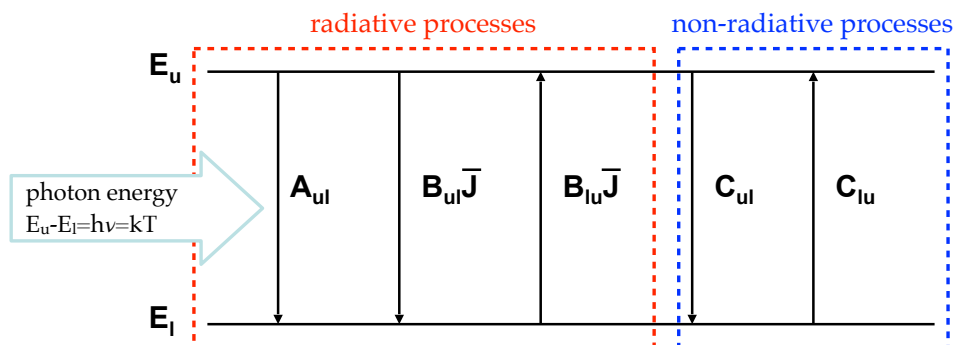
where k is the Boltzmann constant. The upward and downward rates are related through the following:

$$\gamma_{lu} = \gamma_{ul} \frac{g_u}{g_l} e^{-h\nu/kT_k}, \quad (1.3)$$

where g_i is the statistical weight of the i level and T_k is the kinetic temperature. The radiation field is noted in Fig. 1.1 as $\bar{J} = \int_0^\infty J_\nu \Phi(\nu) d\nu$, where J_ν is defined as the integral of the specific intensity I_ν over the source of emission and $\Phi(\nu)$ is the line profile function (Gaussian, Lorentzian...):

$$J_\nu = \frac{1}{4\pi} \int I_\nu d\Omega. \quad (1.4)$$

Figure 1.1: Example of a 2-level system with an upper level energy E_u and a lower level energy E_l .



We need to solve the population rate for each level:

$$\frac{dn_i}{dt} = -n_i \left[\sum_{k < i} A_{ik} + \sum_{k \neq i} (B_{ik} \bar{J} + C_{ik}) \right] + \sum_{k > i} n_k A_{ki} + \sum_{k \neq i} n_k (B_{ki} \bar{J} + C_{ki}), \quad (1.5)$$

¹<https://home.strw.leidenuniv.nl/~moldata/>

²<https://basecol.vamdc.eu/>

where n_i is the population of the energy level i . To solve these equations we need to know the radiation field which is the amount of radiation *inside* the source and which we do not know.

When the energy levels of a molecule are in statistical equilibrium, the rate of transition populating a given energy level is balanced by the rate of transitions which depopulates that same energy level and $\frac{dn_i}{dt} = 0$.

We can derive the Einstein coefficients (A_{ul}, B_{ul}, B_{lu}) by considering a 2-level system and only radiation excitation in Eq. 1.5 with $C_{lu} = C_{ul} = 0$:

$$n_u A_{ul} + n_u B_{ul} \bar{J} = n_\ell B_{lu} \bar{J} \quad (1.6)$$

For a system in thermal equilibrium, the relative level populations follow the Boltzmann distribution:

$$\frac{n_u}{n_\ell} = \frac{g_u}{g_\ell} \exp\left(-\frac{h\nu}{kT}\right), \quad (1.7)$$

where h is the Planck constant, g_u and g_ℓ are the statistical weights of levels up and low respectively and T is the temperature of the region. In non-LTE (Local Thermodynamic Equilibrium), T can be replaced by the so-called excitation temperature. T_{ex} is not a *real* temperature (such as T_k) and corresponds to the temperature for a Boltzmann population in system made of these two levels. This definition is broader than the case of thermal equilibrium and remains valid even if the level population is not at equilibrium. T_{ex} then depends on levels (ℓ, u).

In thermodynamic equilibrium, the radiation field J_ν can be described by the Planck function $B_\nu(T)$:

$$B_\nu(T) = \frac{2h\nu^3}{c^2} \frac{1}{\exp\left(\frac{h\nu}{kT}\right) - 1} \quad (\text{erg s}^{-1} \text{ cm}^{-2} \text{ Hz}^{-1} \text{ sr}^{-1}). \quad (1.8)$$

We can now substitute Eq. 1.7 into Eq. 1.6 to obtain:

$$\bar{J} = \frac{A_{ul}/B_{ul}}{\frac{N_\ell B_{lu}}{N_u B_{ul}} - 1} = \frac{A_{ul}/B_{ul}}{\frac{g_\ell B_{lu}}{g_u B_{ul}} \exp\left(\frac{h\nu}{kT}\right) - 1} \quad (1.9)$$

Comparing Eq. 1.8 with Eq. 1.9 we can now get simplified relationships that allows to express Eq. 1.5 as a function of A_{ul} only:

$$g_u B_{ul} = g_\ell B_{lu}, \quad (1.10)$$

$$A_{ul} = \frac{2h\nu^3}{c^2} B_{ul}. \quad (1.11)$$

Note that some authors use the energy blackbody radiation $U_\nu (=I_\nu(T) \times 4\pi/c)$ instead of J_ν through \bar{J} in Eq. 1.6. A different expression relating the A and B Einstein coefficients is then used: $A_{ul} = B_{ul} \times 8\pi h\nu^3/c^3$. Note however that, in the later definition, only the B coefficients vary, and A is unchanged from one definition to the other. The Einstein coefficient A_{ul} (which are proportional to ν^3) can be found tabulated in the spectroscopic databases such as CDMS³, JPL⁴ and NIST⁵ (see Sec. 3.1).

³<https://cdms.astro.uni-koeln.de/>

⁴<https://spec.jpl.nasa.gov/>

⁵<https://www.nist.gov/pml/observed-interstellar-molecular-microwave-transitions/>

1.1.2 Radiative transfer equation

The intensity of a source emitting in the ISM along a line of sight I_ν , will change if the radiation is absorbed or emitted, and this change can be described by the equation of transfer :

$$\frac{dI_\nu}{ds} = -\alpha_\nu I_\nu + j_\nu, \quad (1.12)$$

where $\frac{dI_\nu}{ds}$ represents the change of the intensity I_ν at the corresponding frequency ν through a slab of material of thickness s . It depends on the absorption coefficient α_ν and the emissivity j_ν [see e.g [Spitzer, 1978](#)]. The expressions of α_ν and j_ν are defined as:

$$\alpha_\nu = \frac{h\nu}{4\pi} (n_\ell B_{\ell u} - n_u B_{u\ell}) \Phi(\nu), \quad (1.13)$$

$$= \frac{c^2}{8\pi\nu^2} \frac{g_u}{g_\ell} n_\ell A_{u\ell} \left(1 - \frac{g_\ell n_u}{g_u n_\ell} \right) \Phi(\nu) \quad (cm^{-1}), \quad (1.14)$$

$$j_\nu = \frac{h\nu}{4\pi} A_{u\ell} n_u \Phi(\nu) \quad (erg\ s^{-1}\ cm^{-3}\ Hz^{-1}\ sr^{-1}). \quad (1.15)$$

Since we do not know the path of propagation s , it is convenient to define a new variable called *optical depth*, or *opacity* of a line at the frequency ν such as:

$$d\tau_\nu = \alpha_\nu ds, \quad (1.16)$$

and define the so-called source function S_ν (Kirchhoff's law of thermal radiation) as:

$$S_\nu = \frac{j_\nu}{\alpha_\nu} = \frac{n_u A_{u\ell}}{(n_\ell B_{\ell u} - n_u B_{u\ell})}. \quad (1.17)$$

Then we get :

$$\frac{dI_\nu}{d\tau_\nu} = -I_\nu + S_\nu, \quad (1.18)$$

$$\frac{dI_\nu}{d\tau_\nu} e^\tau + I_\nu e^\tau = S_\nu e^\tau, \quad (1.19)$$

$$\frac{d}{d\tau_\nu} (I_\nu e^\tau) = S_\nu e^\tau. \quad (1.20)$$

We can then integrate this equation between 0 and τ_ν (cf. Fig. 1.2) :

$$\int_0^{\tau_\nu} \frac{d}{d\tau_\nu} (I_\nu e^\tau) d\tau_\nu = \int_0^{\tau_\nu} S_\nu e^\tau d\tau_\nu, \quad (1.21)$$

$$I_\nu e^\tau - I_\nu(0) = \int_0^{\tau_\nu} S_\nu e^\tau d\tau'_\nu, \quad (1.22)$$

$$I_\nu = I_\nu(0) e^{-\tau} + \int_0^{\tau_\nu} S_\nu \exp[-(\tau_\nu - \tau')] d\tau', \quad (1.23)$$

where $I_\nu(0)$ represents the background radiation, i.e the cosmic microwave background (CMB) at 2.7 K.

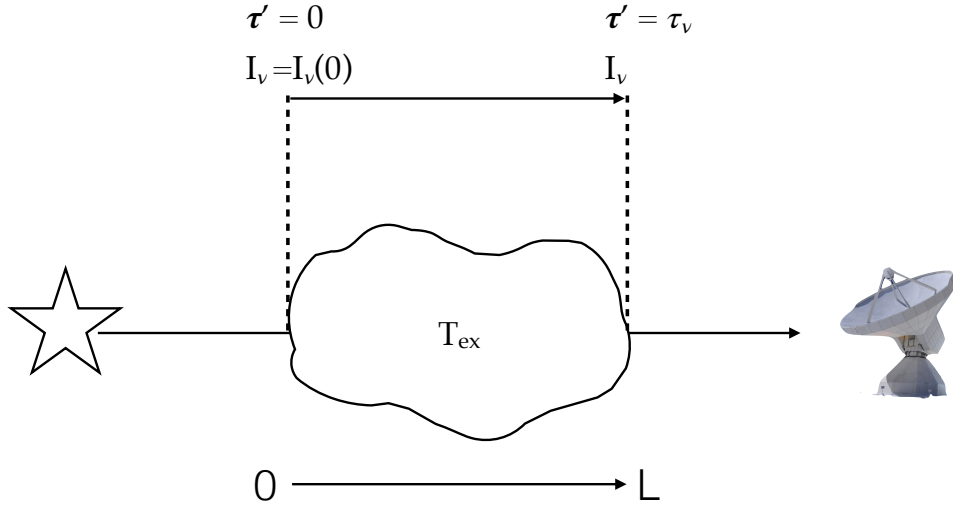


Figure 1.2: Passage of a beam through a gaseous object of length L , excitation temperature T_{ex} .

Assuming that the source function does not vary in the observed medium at a constant temperature (it does not vary as a function of the opacity), we then get :

$$I_\nu = I_\nu(0)e^{-\tau_\nu} + S_\nu(1 - e^{-\tau_\nu}). \quad (1.24)$$

From this equation we can consider two cases depending on the optical depth of the medium:

- $\tau \ll 1$, hence $I_\nu = I_\nu(0)$, the total emission is equal to the background emission,
- $\tau \gg 1$ hence $I_\nu = S_\nu$, the total emission is equal to the source function.

In order to compare the intensity of the observed signal with the original intensity of the emitting source in absence of the intervening ISM ($I_\nu(0)$), we get :

$$I_{\nu_{obs}}(s) = I_\nu(s) - I_\nu(0) = (S_\nu(T) - I_\nu(0))(1 - e^{-\tau_\nu}). \quad (1.25)$$

The Source function is equivalent to the Planck function at the temperature T_{ex} : $S_\nu = B_\nu(T_{ex})$ (see Eq. 1.8 and Eq. 1.17). Equation 1.25 can then be rewritten as:

$$I_{\nu_{obs}} = \frac{2h\nu^3}{c^2} \left[\frac{1}{e^{h\nu/kT_{ex}} - 1} - \frac{1}{e^{h\nu/kT_{CMB}} - 1} \right] (1 - e^{-\tau_\nu}). \quad (1.26)$$

The radiation $I_{\nu_{obs}}$ is defined by the Planck's function at T_b ($I_{\nu_{obs}} = B_\nu(T_b)$), the brightness temperature of the source (in K). In the Rayleigh-Jeans (RJ) limit (namely $\frac{T_0}{T} \ll 1$ where $T_0 = h\nu/k$),

$$I_\nu = \frac{2k\nu^2 T_b}{c^2}. \quad (1.27)$$

It is the custom in radioastronomy to measure the brightness of a source by its brightness temperature, T_b . The RJ limit stands for frequencies ν (in GHz) $\ll 20.84 \times T$ (in K), and it is valid for radio emission except perhaps for the low temperatures (cold cores of about 10 K). When ν is so high that RJ does not stand, Eq. 1.27 can still be used but in this case but it should be understood that in this case, T_b is different than the thermodynamic temperature of a blackbody.

The Equation 1.26 can be expressed as :

$$T_b(\nu) = T_0 \left(\frac{1}{e^{T_0/T_{ex}} - 1} - \frac{1}{e^{T_0/T_{CMB}} - 1} \right) (1 - e^{-\tau(\nu)}), \quad (1.28)$$

where $T_0 = h\nu/k$. One might apply the filling factor correction η (lying between 0 and unity) as a multiplicative factor to Eq. 1.26 [see Ulich and Haas, 1976]:

$$\eta = \frac{\Omega_{source}}{\Omega_{observed}}, \quad (1.29)$$

where Ω is the solid angle. We assume for single dish observations, that the telescope beam Full Width Half maximum (FWHM) size is related to the diameter of the telescope by the diffraction limit:

$$\theta_b = 1.22 \frac{\lambda}{D}, \quad (1.30)$$

where θ_b is the angular resolution (radians), λ is the wavelength of light, and D is the diameter of the telescope. The gaussian beam is frequently used in formula deduction for single dish. The size of a gaussian beam is characterised by Half Power Beam Width of the main lobe: θ_b . The solid angle of such a gaussian beam is:

$$\Omega_b = \int e^{-4 \times \ln(2) \times \left(\frac{\theta^2}{\theta_b^2}\right)} \times 2\pi \times \theta d(\theta) = \frac{\pi}{4 \times \ln(2)} \times \theta_b^2 = 1.133 \times \theta_b^2. \quad (1.31)$$

Therefore, the filling factor can be expressed as:

$$\eta = \frac{\theta_{source}^2}{\theta_{source}^2 + \theta_{beam}^2} \quad (1.32)$$

where θ_{source} and θ_b are the circular 2D Gaussian sizes of the source (if centered in the telescope beam) and half-power telescope beam respectively. For example, with a 10'' source size and a 10'' telescope beam, we still get a factor 1/2 for the filling factor to be applied to Eq. 1.28. A non-gaussian intensity distribution requires to work out more closely the relation between the telescope response (beam) and the source intensity distribution. Indeed, if not centered, the measured intensity is attenuated with respect to the intrinsic intensity.

When a background continuum source (T_{dust}, τ_{dust}) is coupled to the molecular/atomic cloud (T_{ex}, τ) along the line of sight (see Fig. 1.3), the previous equation must take into account the dust temperature and opacity, as well as the cosmic microwave background (CMB). In an ON-OFF observation, the resulting brightness temperature obtained from

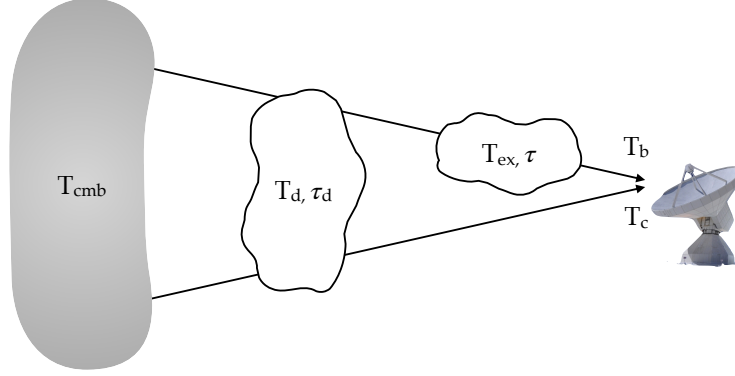


Figure 1.3: Sketch of multiple clouds along the line of sight. The brightness temperature of the cloud is T_b and the one of the continuum is T_c .

the telescope is :

$$T_b = J_\nu(T_{CMB})e^{-\tau_{dust}}e^{-\tau} + \eta_{dust}J_\nu(T_{dust})(1 - e^{-\tau_{dust}})e^{-\tau} + \eta J_\nu(T_{ex})(1 - e^{-\tau}) - J_\nu(T_{CMB}), \quad (1.33)$$

where $J_\nu(T) = (h\nu/k) \times 1/(e^{h\nu/kT} - 1)$ is the radiation temperature, η_{dust} represents the filling factor for the continuum source and η represents the dilution factor for the molecular/atomic cloud. In the case where $\tau_{dust} = 0$ and $\eta = 1$, the equation becomes :

$$T_b = (J_\nu(T_{ex}) - J_\nu(T_{CMB}))(1 - e^{-\tau}). \quad (1.34)$$

In the case where $\eta = \eta_{dust} = 1$, then:

$$T_b = (J_\nu(T_{CMB})e^{-\tau_{dust}} + J_\nu(T_{dust})(1 - e^{-\tau_{dust}}))e^{-\tau} + J_\nu(T_{ex})(1 - e^{-\tau}) - J_\nu(T_{CMB}). \quad (1.35)$$

Outside the line, towards the continuum source, the continuum obtained in the ON-OFF observation is defined by:

$$T_c = (J_\nu(T_{CMB})e^{-\tau_{dust}} + J_\nu(T_{dust})(1 - e^{-\tau_{dust}})) - J_\nu(T_{CMB}). \quad (1.36)$$

Combining Eq. 1.35 and 1.36 give a resulting brightness temperature :

$$T_b = T_c \times e^{-\tau} + (1 - e^{-\tau})(J_\nu(T_{ex}) - J_\nu(T_{CMB})). \quad (1.37)$$

- For emission lines:

$$T_b - T_c = \Delta T = (1 - e^{-\tau})(J_\nu(T_{ex}) - J_\nu(T_{CMB}) - T_c). \quad (1.38)$$

- For absorption lines:

$$T_c - T_b = T_{abs} = (1 - e^{-\tau})(T_c - J_\nu(T_{ex}) + J_\nu(T_{CMB})). \quad (1.39)$$

Several components (spatially distributed, with different V_{LSR} and/or temperature/density) and molecules can be modelled at the same time. For each molecules, several transitions can be modelled within the spectrum. The spectra of these components are computed separately, and then added iteratively. In the following equations, the indices i , j and k correspond to components, molecules, and lines, respectively. The spectrum is computed in a first iteration with the first component:

$$T_{b,0}(\nu) = T_c(\nu)e^{-\sum_{j,k}\tau_{0,j,k}(\nu)} + \sum_j \eta_{0,j} \left(1 - e^{-\sum_k\tau_{0,j,k}}\right) (J_\nu(T_{ex,0,j,k}) - J_\nu(T_{bg})) . \quad (1.40)$$

The other components are then added iteratively in the case of an onion-like structure:

$$T_{b,i=[1,N-1]}(\nu) = T_{b,0}(\nu)e^{-\sum_{j,k}\tau_{i,j,k}(\nu)} + \sum_j \eta_{i,j} \left(1 - e^{-\sum_k\tau_{i,j,k}}\right) (J_\nu(T_{ex,i,j,k}) - J_\nu(T_{bg})) . \quad (1.41)$$

The continuum emission is here assumed to be optically thin (i.e. transparent to the CMB) and spatially uniform, to fill the beam of the single-dish telescope or the synthesised beam of the interferometer. In LTE, $T_{ex,i,j,k}$ has the same value within each component (i) for each transition (k).

1.2 Molecular column densities

In CASSIS, you can provide, in LTE, the column density, excitation temperature, the line width and the source size and it will compute the filling factor, the opacity and then it will reconstruct the line profile using for example a Gaussian profile. In non-LTE, you can provide the column density, the kinetic temperature, the density of the collider, the line width and the source size and it will compute the filling factor, the opacity and then it will reconstruct the line profile using for example a Gaussian profile.

1.2.1 Opacity

In order to derive the physical conditions of the observed medium, it is useful to measure the number of molecules per unit area along the targeted line of sight. This quantity is called the molecular column density and is the first step before measuring the molecular abundances (in LTE) or the kinetic temperature, collider density and molecular abundances (in non-LTE). We can express the column density in i level, N_i as a function of the number of molecules in the energy level i (n_i : number per cm^{-3}):

$$N_i = \int_0^L n_i ds , \quad (1.42)$$

L being the size of the source along the line-of-sight, and ds the infinitesimal element of length along the line-of-sight. The line opacity can be expressed as a function of the column density and the excitation temperature, that we assume to be constant on the

line of sight. For that we can integrate τ along the line profile :

$$\int \tau_\nu d\nu = \int \frac{h\nu\Phi_\nu}{4\pi} (B_{lu}N_l - B_{ul}N_u) d\nu \quad (1.43)$$

$$= \frac{A_{ul}c^3 N_u}{8\pi\nu^3} (\exp(h\nu/kT_{ex}) - 1), \quad (1.44)$$

Where Φ_ν is the line profile with $\int \Phi(\nu)d\nu=1$. For a gaussian line shape, we can express the opacity (Eq. 1.16) as a function of the cloud's depth :

$$\tau_{ul}(z) = \frac{A_{ul}c^2}{8\pi\nu^3 \Delta\nu \sqrt{\pi}/2\sqrt{\ln 2}} \int_0^z n_u \left(\frac{n_l g_u}{n_u g_l} - 1 \right) dz', \quad (1.45)$$

where $\Delta\nu$ (velocity units) is the full width at half maximum of the observed line. Integrating on the line of sight (see equation 1.42), we get, at the line center :

$$\tau_0 = \frac{g_u}{g_l} \frac{c^2}{8\pi\nu^2 \Delta\nu \sqrt{\pi}/2\sqrt{\ln 2}} A_{ul} N_l (1 - e^{-h\nu/kT_{ex}}), \quad (1.46)$$

where $\Delta\nu$ (frequency units) is the FWHM of the observed line, and N_l is the column density in the lower state.

This equation can also be expressed as:

$$\tau_0 = \frac{c^2 A_{ul} N_u}{8\pi\nu^2 \Delta\nu \sqrt{\pi}/2\sqrt{\ln 2}} (e^{h\nu/kT_{ex}} - 1). \quad (1.47)$$

The next step is now to estimate the total column density of the observed molecular species, not just the column density in an energy level. Statistical mechanics states that, when the gas exchange energy with the ambient medium, the partition function Q describes the relative population of states in the gas as:

$$Q(T) = \sum_i g_i \exp\left(-\frac{E_i}{kT}\right). \quad (1.48)$$

The partition function is a function of the nuclear spin, rotational, vibrational, electronic states of the molecule: $Q = Q_n Q_r Q_v Q_e$ (see [Gordy and Cook \[1984\]](#) and [Mangum and Shirley \[2015\]](#)).

The total column density N_{tot} can then be computed as a sum on all levels:

$$N_{tot} = \sum_{n=0}^{\infty} N_n. \quad (1.49)$$

Using equation 1.48 we can now express the total column density:

$$N_{tot} = \frac{N_{lowest} Q(T_{ex})}{g_{lowest}} = \frac{N_u Q(T_{ex}) e^{E_u/kT_{ex}}}{g_u}, \quad (1.50)$$

where $Q(T_{ex})$ is the partition function for an excitation temperature T_{ex} and the index *lowest* represents the lowest level associated to the molecule and its form (ortho, para, A,

E: see 3.2). Indeed, in the case of the water molecule, the lowest energy level for the para form is 0 K and 34.23 K for ortho. E_u is the upper level of the transition compared to the ground level (different from zero when ortho, para or meta forms).

Combining Eq. 1.47 and Eq. 1.50, we finally obtain:

$$N_{tot} = \frac{Q(T_{ex})e^{E_u/kT_{ex}}}{g_u} \times \frac{\tau_0 8\pi \left(\frac{\sqrt{\pi}}{2\sqrt{\ln(2)}} \right) \nu^2 \Delta\nu}{c^2 A_{ul}(e^{h\nu/kT_{ex}} - 1)} \quad (1.51)$$

where τ_0 is the opacity at the line centre, derived from the maximum intensity at the line peak emission (see Eq. 1.28).

When the collision rate between molecules is high, $T_{ex} \rightarrow T_b \rightarrow T_K$. By choosing a column density such that $\tau \gg 1$ at the line center, the line will therefore saturate, the temperature at the line center will become constant, and will result in a non-negligible line broadening (see Eq. 1.28).

Figure 1.4 presents the modelled line profiles of the ^{12}CO molecule for transitions $1 \rightarrow 0$ and $2 \rightarrow 1$ at $T_{ex} = 20$ K, FWHM = 1 km s $^{-1}$, $\tau = 10$ and $\tau = 0.5$ at the line center. We assume a gaussian profile:

$$\tau(\nu) = \tau_0 \exp\left(-\frac{(\nu - \nu_0)^2}{2\sigma^2}\right), \quad (1.52)$$

where ν_0 is the velocity in the local standard of rest (V_{LSR}), $\sigma(\text{km/s}) = \Delta\nu (\text{km/s}) / (2\sqrt{2\ln 2})$, where $\Delta\nu$ is the FWHM. Using Eq. 1.28 we get $T_b = 16.5$ K for the $1 \rightarrow 0$ transition and $T_b = 14.8$ K for the $2 \rightarrow 1$ transition. Note that in LTE, $T_{ex} = T_k$, then in the RJ limit with $\tau \gg 1$, $T_b \approx T_k - T_{CMB}$. Therefore T_b measured at the peak (Fig. 1.4) gives a direct measure of T_k . In this case, at 115 GHz, $h\nu/kT \ll 1$, but not at 230 GHz, and $T_{ex} = T_k = 16.7 + 2.73 \approx 20$ K, which is consistent with the value given as an input for the model. We can see that for low opacity the profile follows a Gaussian profile, and increasing the opacity tends to saturate the line profile, deviating from a Gaussian one.

In the LTE regime, proper estimation of T_{ex} requires the observation of multiple transitions (many upper energy levels covering at least the temperature range of the observed source) coupled with modelling of the statistical equilibrium and radiative transfer. The gas excitation temperature varies between the background radiation temperature (T_{CMB} when no background is present) at low density and the gas kinetic temperature at high density. At low densities, collisions are not the dominant excitation mechanisms and T_{ex} is in equilibrium with the radiation temperature. It can be demonstrated from Eq. 1.6, combined with Eq. 1.7 and Eq. 1.8 with $B_\nu(T_{CMB})$. At high densities, collisions dominate in setting the level population and T_{ex} is equal to the gas kinetic temperature of the dominant collisional partner. It can be demonstrated from Eq. 1.5, neglecting the radiative terms:

$$n_u(A_{ul} + B_{ul}\bar{J} + C_{ul}) = n_\ell(B_{\ell u}\bar{J} + C_{\ell u}). \quad (1.53)$$

Therefore,

$$n_u C_{ul} = n_\ell C_{\ell u}. \quad (1.54)$$

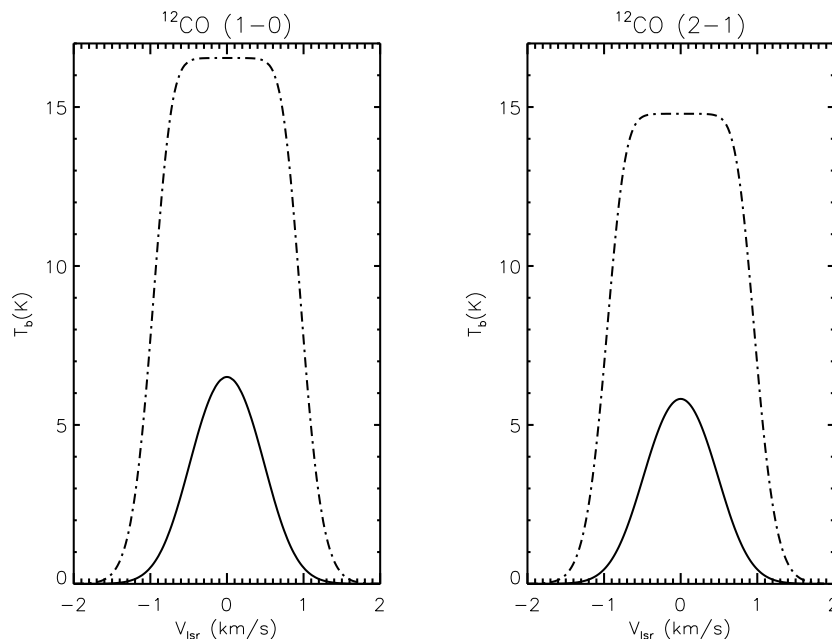


Figure 1.4: Line profiles for the ^{12}CO transitions $1 \rightarrow 0$ and $2 \rightarrow 1$ at $T_{ex} = 20$ K, $\Delta v = 1$ km s $^{-1}$ and the opacity $\tau = 0.5$ (plain lines) and 10 (dot-dashed lines) at the line centre using CASSIS.

Using Eq. 1.3 and 1.7, the excitation temperature tends to reach the kinetic temperature and the transition is *thermalised* (i.e LTE). We say that the line is sub-thermally excited when T_{ex} is less than T_k . Note that some transitions of the same molecule can be thermalised (for example the CO 1–0 transition) while higher energy levels are sub-thermally excited.

We can now introduce a new parameter, called the *critical density* (n_{cr}), which has traditionally been used as a measure of the density at which a particular transition is excited and is observed at radio wavelengths. The definition of the critical density is unfortunately not consistent throughout the literature. Some definitions only consider the two energy levels involved in the transition (2-level approximation):

$$n_{cr}(ul) = \frac{A_{ul}}{\gamma_{ul}}, \quad (1.55)$$

where γ_{ul} depends on the kinetic temperature. It defines the density of the gas required for the collisions to dominate over the radiative processes. Other definitions use the multi-level nature of collisions to sum over all collisions out of the upper energy level or only from the upper energy level to lower energy levels [see for example Shirley, 2015]. From Eq. 1.55, the critical density is defined for each transition and is proportional to ν^3 , so the higher the upper energy is, the higher the frequency, therefore the Einstein coefficient and the critical density. As an example, using the LAMDA catalog, the critical density of $\text{HC}_3\text{N } J = 9-8$ at 81.88 GHz is $n_{cr} = [2.8 - 7.0] \times 10^5$ cm $^{-3}$ ($E_u = 19.6$ K, A_{9-8}

$= 4.2 \times 10^{-5} \text{ s}^{-1}$, $\gamma_{9-8} (10 - 300 \text{ K}) = [5.97 \times 10^{-11} - 1.51 \times 10^{-10}] \text{ cm}^3 \text{ s}^{-1}$. At 336.52 GHz, the critical density of $\text{HC}_3\text{N } J = 37-36$ is $n_{cr} = [8.4 - 27.7] \times 10^6 \text{ cm}^{-3}$ ($E_u = 306.9 \text{ K}$, $A_{37-36} = 3.05 \times 10^{-3} \text{ s}^{-1}$, $\gamma_{37-36} (10 - 300 \text{ K}) = [1.11 \times 10^{-10} - 3.62 \times 10^{-10}] \text{ cm}^3 \text{ s}^{-1}$). Therefore, the higher-frequency transitions are more readily sub-thermally excited. In contrast, the CO 1–0 and 2–1 transitions have much lower critical densities but are easily observed from the ground and detected (high Einstein coefficients) in the ISM, as the second most abundant molecule. These CO transitions are therefore good tracers of molecular gas in our Galaxy and beyond [see e.g. Liszt and Lucas, 1998, Dame et al., 2001, Goldsmith et al., 2008]. However it should be noted that the use of CO has some caveats: 1) the low-J CO lines become easily optically thick (the 1–0 transition becomes optically thick beyond 10^{16} cm^{-2} , which corresponds to a few visual extinction [Liszt and Lucas, 1998] so that they cannot directly probe the highest density regions; 2) at low column densities, CO is rapidly photodissociated by the interstellar radiation field [van Dishoeck and Black, 1988]. That is why there have been a lot of effort to detect higher density tracers such as HCO^+ , N_2H^+ , HCN, HC_3N , NH_3 , although with much weaker line intensities compared to CO or even CS. Note that the high-J CO lines detected in the submm/infrared may be optically thin.

Going back to the Fig. 1.4 line profiles, several mechanisms can broaden spectral lines. The dynamical structure of the source, if unresolved, may contribute to such broad lines such as outflows, collapsing envelopes, stellar winds, etc...Also, individual atoms in a gaseous medium are in random, chaotic motion: the hotter the gas, the faster the random thermal motions of the atoms. When a photon is emitted by an atom in motion, the frequency of the detected photon is changed by the Doppler effect. The photon is then not recorded at the precise frequency predicted by atomic physics but rather at a slightly shifted. Throughout the whole cloud, atoms move in every possible direction, resulting in a broadening of the line. From Fuller and Myers [1992]:

$$(\Delta v)^2 = 8 \ln(2) \frac{kT}{m}, \quad (1.56)$$

where Δv is the FWHM, T is temperature in the gas, and m is the mass of the atom (or molecule). For example, in the case of the D_2H^+ molecule, at a temperature of 8 K, the thermal linewidth should be 0.27 km s^{-1} . Note that turbulence can also result in the broadening of a spectral line.

By defining a column density and an excitation temperature, we get from 1.43 $\int \tau dv$. Then, using a linewidth (before broadening due to optical depth), we get $\tau(v)$ (as a function of velocity), which has a Gaussian profile (Eq. 1.52). Then from 1.28 we get T_b as a function of velocity. Different line profiles can therefore be used.

1.2.2 LTE Rotational diagram analysis

This analysis refers to a plot of the column density per statistical weight of a number of molecular energy levels, as a function of their energy above the ground state (see Goldsmith and Langer [1999]). In LTE, this corresponds to a Boltzmann distribution, so

a plot of the natural logarithm of N_u/g_u versus E_u/k yields a straight line with a slope of $-1/T_{rot}$. The temperature inferred is called the rotation temperature.

We can rewrite Eq. 1.47 as:

$$\tau = \frac{c^3 A_{ul} N_u}{8\pi\nu^3 \Delta\nu \sqrt{\pi}/2\sqrt{\ln 2}} [e^{h\nu/kT_{rot}} - 1]. \quad (1.57)$$

Neglecting $J_\nu(T_{CMB})$ from Eq. 1.28 compared to $J_\nu(T_{rot})$, which means $T_{CMB} \ll T_{rot}$, we can express the main beam temperature as:

$$T_b = \frac{h\nu}{k} \frac{1}{\exp(h\nu/kT_{rot}) - 1} \frac{1 - e^{-\tau}}{\tau} \times \tau. \quad (1.58)$$

Therefore, we can compute the column density in the upper state as:

$$N_u = \int T_b d\nu \times \frac{8\pi k\nu^2}{hc^3 A_{ul}} \times \frac{\tau}{1 - e^{-\tau}}. \quad (1.59)$$

$$N_u = W \times \frac{8\pi k\nu^2}{hc^3 A_{ul}} \times C_\tau, \quad (1.60)$$

where W in the integrated area and C_τ is the optical depth correction factor. When the line is optically thin, C_τ is equal to unity.

For a molecule in LTE, all excitation temperatures are the same, and the population of each level is given by:

$$N_u = \frac{N_{tot}}{Q(T_{rot})} g_u e^{-E_u/kT_{rot}}. \quad (1.61)$$

We can rewrite this equation to obtain:

$$\ln \frac{N_u}{g_u} = \ln \frac{N_{tot}}{Q(T_{rot})} - \frac{E_u}{kT_{rot}}. \quad (1.62)$$

A rotational diagram can be useful to determine whether the emission is optically thick or thin, whether the level populations are described by LTE, and to determine what temperature describe the population distribution in the event that LTE applies. Equation 1.62 can be written in terms of the observed integrated area W (K km s^{-1}):

$$\ln \frac{8\pi k\nu^2 W}{hc^3 A_{ul} g_u} = \ln \frac{N_{tot}}{Q(T_{rot})} - \ln C_\tau - \frac{E_u}{kT_{rot}}. \quad (1.63)$$

If we do not take into account the C_τ factor, each of the upper level populations would be underestimated by a factor C_τ , different for each transition. Therefore, the ordinate of the rotation diagram would be below its correct value by the factor $\ln C_\tau$. A change in the temperature for lines of different excitation might indicate that the source has different temperature components or that the lines considered are not optically thin and cannot be easily used to obtain a meaningful excitation temperature.

Note that the error bars should be taken into account for the order 1 polynomial fit, in order to obtain a reliable value for the uncertainty on the rotational temperature as well

as the total column density. The uncertainty of the integrated area is computed through the following formula:

$$\Delta W = \sqrt{(cal/100 \times W)^2 + (rms\sqrt{2 \times FWHM \times \delta v})^2}, \quad (1.64)$$

where cal is the instrumental calibration uncertainty (%), W is the integrated area (in K km s⁻¹), rms is the noise around the selected species (in K), FWHM is expressed in km s⁻¹ and δv is the bin size (in km s⁻¹). We assumed that the number of channels in the line is $2 \times FWHM/\delta v$. For undetected transitions we estimated the upper limit of 3σ :

$$W \text{ (K km s}^{-1}\text{)} \leq 3(rms \times FWHM) \times \sqrt{(2 \times \alpha)^2 + (2 \times \delta V/FWHM)}. \quad (1.65)$$

Therefore, the plotted uncertainties are simply:

$$\Delta \left(\ln \frac{N_u}{g_u} \right) = \frac{\Delta W}{W}. \quad (1.66)$$

Now, how do we estimate the uncertainty on the values of T_{rot} and N_{tot} ? From the fitted straight line ($y = ax+b$) the slope a is related to the rotational excitation temperature as $T_{rot} = -1/a$. Then $\Delta T_{rot} = \Delta a/a^2$. The intercept b is related to the total column density as $N_{tot} = Q(\text{rot}) \times e^b$. Therefore $\Delta N_{tot} = Q(\text{rot}) \times \Delta b \times e^b$.

We can iteratively apply the C_τ correction to the rotational diagram analysis until a solution for T_{rot} and N_{tot} has converged (when the last result has not changed by a small value). For the first iteration we use Equation 1.62 and obtain values for the transitions opacity. In the second iteration we add the C_τ correction to the linear equation:

$$\ln \frac{N_u}{g_u} = \ln \frac{N_{tot}}{Q(T_{rot})} - \frac{E_u}{kT_{rot}} - \ln C_\tau. \quad (1.67)$$

The iterations go on until a convergence has been obtained.

As Goldsmith and Langer (1999) nicely said, this method requires quite a large number of transitions spread over a range of upper state energies.

Please note that between Eq. 1.57 and Eq. 1.58, $J_\nu(T_{CMB})$ has been neglected from Eq. 1.28 compared to $J_\nu(T_{rot})$. Therefore the above analysis does not stand when T_{CMB} is not negligible compared to T_{rot} .

CASSIS provides the values for the column density, excitation temperature and the corresponding errors, reduced χ^2 and the probability of occurrence (P value) for a χ^2 value depending on degrees of freedom. The degree of freedom in our linear fit corresponds to the number on points (n) on which the fit was performed minus 2 (2 values extracted from the fit: N and T_{ex}).

The method of least squares states that the best values are those for which S is minimized:

$$S = \sum_{i=1}^n \frac{(y_i - y)^2}{\sigma^2} = \sum_{i=1}^n \frac{(y_i - ax_i - b)^2}{\sigma_i^2} \quad (1.68)$$

Ideally S is expected to follow a chi-square distribution with its mean value equal to the degrees of freedom (dof). We thus expect S to be close to $dof = n - 2$ if the fit is good. A quick and easy test is to form the reduced chi-square χ^2/dof which should be close to 1 for a good fit. A more rigorous test is to look at the probability of obtaining a χ^2 value greater than S , i.e., $P(\chi^2 \geq S)$. This requires integrating the χ^2 distribution or using cumulative distribution tables. In general, if $P(\chi^2 \geq S)$ is greater than 5%, the fit can be accepted. This probability is just a tool for deciding whether to reject or validate the fit as frequentist statistics does not, and cannot, attach probabilities to hypotheses. An important point to consider is when S is very small. This implies that the points are not fluctuating enough. Beyond falsified data, the most likely cause is an overestimation of the errors on the data points. Indeed, the error bars represent a 1σ deviation, so that about 1/3 of the data points should be expected to fall outside the fit. If the errors have been under-estimated then an improbably high value of χ^2 can be obtained.

CASSIS provides the reduced χ^2 and the probability $P(\chi^2 \geq S)$. Values of the χ^2 or reduced χ^2 corresponding to the probability $P(\chi^2; dof=2)$ of exceeding χ^2 can be found in the literature [e.g. [Bevington and Robinson, 2003](#)]. Since the true probability of the data being consistent with the model depends on both χ^2 and dof , we decided to provide the reduced χ^2 and the probability so that the user decides on the goodness of its fit. For example, if we obtain a value of $\chi^2 = 1.95$ for 7 degrees of freedom, the corresponding probability is about 96%. Although this probability may seem to be gratifyingly high, the very low value of χ^2 gives a strong indication that the common uncertainty in the data may have been overestimated.

If you plan on performing a population diagram analysis on 2 points only, CASSIS will evidently not be able to provide the errors on the column density and excitation temperature nor the χ^2 and probability values. Two points can always be fitted by a straight line.

Note that CASSIS can perform the rotational diagram analysis assuming optically thin lines for multiplet transitions (\sim same frequency, \sim same upper energy), but not on blended transitions (\sim same frequency, different upper energy). However the opacity correction cannot be performed on both for the moment. After using the Rotational Diagram module within CASSIS, I suggest that you use the column density and excitation temperature values in the Line Analysis module in order to compare the synthetic spectrum with your observations. **Note that CASSIS provides a [python script with many options that will produce a publishable figure such as Fig. 1.5](#)**. It uses the output of the fit performed in the *Rotational Diagram module*, under the *Save* tab: Save displayed values and Save fit values.

1.2.3 Non-LTE formalism

When the LTE conditions are not fulfilled, the C_{ul} and C_{lu} collisional coefficients cannot be neglected and Eq. 1.5 must be solved. Some simplifications must be done. The problem is how to *decouple* the radiative transfer calculations from the calculations of the level populations. A popular approach for this is the so-called escape probability

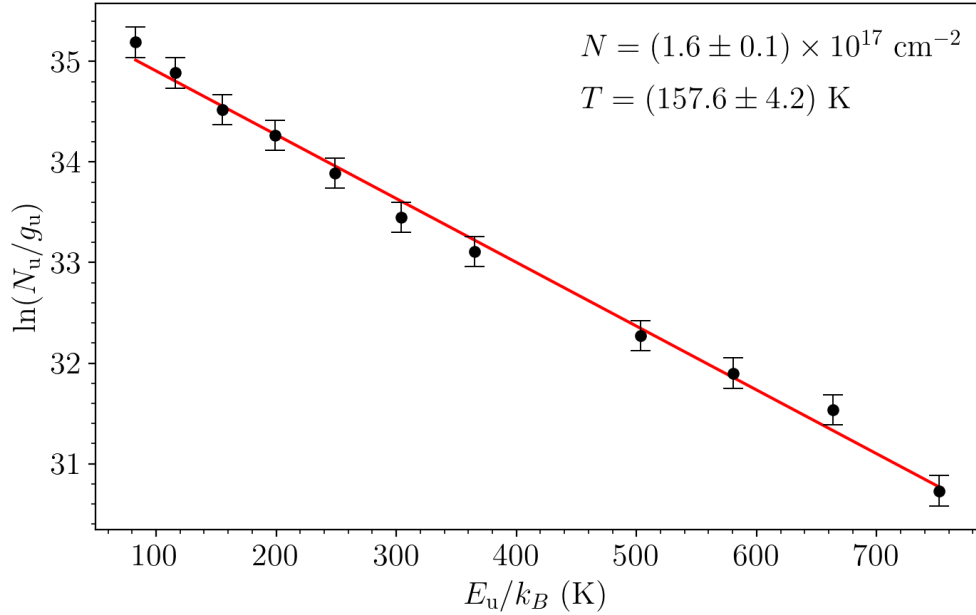


Figure 1.5: Rotational diagram analysis using CASSIS and its python script for the CO detected transitions using Herschel/HIFI towards the Orion Bar. The opacity correction has been applied. The CO column density and rotational temperature are quoted in the upper right corner. No beam dilution has been taken into account.

method (described by Sobolev [1960]). A factor (β) that determines the probability that a photon at some position in the cloud can escape the system is introduced in the equations 1.5: $\bar{J}_\nu = S_\nu(1 - \beta)$. Indeed, locally, the number of photons used for absorptions ($(n_\ell B_{\ell u} - n_u B_{u\ell})\bar{J}$) is equal to the number of photons available for local absorption and therefore not escaping the cloud ($n_u(1 - \beta(\tau_{u\ell}))A_{u\ell}$). Now the statistical equilibrium equations can take a much easier form:

$$\frac{dn_u}{dt} = n_\ell C_{\ell u} - n_u C_{u\ell} - \beta n_u A_{u\ell}. \quad (1.69)$$

So now we can solve the level populations and the radiation field separately as they are now decoupled. We can then estimate the escape probability value.

A first expression of β has been derived for an expanding spherical sphere by Sobolev [1960] and also applies to moderate velocity gradients. It is called the Large Velocity Gradient (LVG) approximation (also called Sobolev) in which Castor [1970] and Elitzur [1992] (Chapter 2) derived:

$$\beta = \frac{1 - e^{-\tau}}{\tau}. \quad (1.70)$$

For a uniform sphere, Osterbrock and Ferland [2006] derived:

$$\beta = \frac{1.5}{\tau} \left[1 - \frac{2}{\tau^2} - \left(\frac{2}{\tau} + \frac{2}{\tau^2} \right) e^{-\tau} \right]. \quad (1.71)$$

For a homogeneous slab geometry, also applicable to shocks, [de Jong et al. \[1975\]](#) derived:

$$\beta = \frac{1 - e^{-3\tau}}{3\tau}. \quad (1.72)$$

When the gas becomes optically thick ($\tau \gg 1$), the probability for a photon to escape the medium is considerably reduced, because of the *trapping* of emitted photons. In this case, the effective rate of spontaneous emission has to be reduced by the number of photons leaving the system: $A_{ul}^{eff} = A_{ul}\beta(\tau)$. Hence the critical density is now described by:

$$n_{cr}^{eff}(u\ell) = \frac{A_{ul}\beta(\tau)}{\gamma_{ul}}. \quad (1.73)$$

This situation leads to more easily thermalised molecular levels since the n_{cr} leading to thermalisation is reduced ($\beta(\tau) < 1$). The resolution of the LVG method is quite similar to the LTE method except that the term A_{ul} is replaced by $A_{ul}\beta(\tau)$ and the term \bar{J}_ν is replaced by $S_\nu(1 - \beta)$ in the equations. We can write:

$$n_\ell n_{collider} \gamma_{\ell u} = n_u (n_{collider} \gamma_{ul} + \beta A_{ul}). \quad (1.74)$$

Combined with Eq. 1.3 we obtain:

$$\frac{n_u}{n_\ell} = \frac{g_u}{g_\ell} \frac{e^{-h\nu_0/kT_k}}{\frac{\beta A_{ul}}{n_{collider} \gamma_{ul}} + 1} = \frac{g_u}{g_\ell} \frac{e^{-h\nu_0/kT_k}}{\frac{n_{cr}^{eff}}{n_{collider}} + 1}. \quad (1.75)$$

Taking into account the Boltzmann equation (Eq. 1.7) we obtain:

$$T_{ex} = \frac{T_k}{1 + \frac{kT_k}{h\nu_0} \ln \left(\frac{n_{cr}^{eff}}{n_{collider}} + 1 \right)}. \quad (1.76)$$

If $n \gg n_{cr}^{eff}$, hence $T_{ex} = T_k$ and the line is thermalised (LTE case).

Equation 1.69 can then be solved for each level assuming equilibrium, computing T_{ex} for each level (Eq. 1.76), then the opacity (Eq. 1.47) then the integrated line intensity (from Eq. 1.28). As a first guess, we consider the level populations in the optically thin case and we solve n_i . Then we compute τ and then β , which we re-inject into the equilibrium equations to solve n_i (and therefore N_i) and T_{ex} for each transition. We can then iterate the procedure and stop when the values do not change. The unknown parameters are therefore the kinetic temperature of the medium, the number density of the collider, the column density of the molecular species and the width of the transitions (assumed to be same for all the transitions of the same species). These can be constrained when a few transitions of the same species have been detected. Large modelling grids can be computed and a χ^2 minimisation can be used to match the integrated intensities of the observed transitions:

$$\chi^2 = \sum_{i=1}^N \frac{(W_i^{obs} - W_i^{mod})^2}{(cal/100 \times W_i^{obs})^2 + (rms\sqrt{2} \times fwhm \times \delta\nu)^2} \quad (1.77)$$

where N is the number of observed lines, W_i^{obs} is the observed integrated line intensity, W_i^{mod} is the modelled integrated line intensity such as provided with RADEX (see Chap. 2), cal is the instrumental calibration uncertainty (%), rms is the noise around the selected transitions (in K), FWHM is expressed in km s^{-1} and $\delta\nu$ is the bin size (in km s^{-1}).

1.3 Abundances

Molecules can be used as probes of the physical (kinetic temperature and H_2 density as well as motions such as collapse or rotation) and chemical (abundances) information on the gas. In order to properly determine the abundances of the detected species, it is mandatory to determine the H_2 column density. In molecular clouds, H_2 produced on the dust grain surfaces and ejected in the gas-phase cannot be directly traced. Indeed, it is a homonuclear linear molecule with no permanent dipole moment, and all of the low-lying energy levels are quadrupole transitions with small transition probabilities (A_{ul} values) and relatively high excitation energies. These transitions are therefore only excited at high temperatures or in strong UV radiation fields (i.e., fluorescence). The generally high energies of the first excited states of H_2 mean that we expect negligible H_2 emission unless we are looking at unusually warm (500–1000K) gas in proximity to hot stars or in regions of active star formation. Consequently the most abundant molecule in the ISM, carrying most of the mass and playing a key role for the thermal balance and gas-phase chemistry of the ISM, is virtually invisible to direct observation. In this section, we review the methodology leading to the determination of the abundances of the observed molecular species.

1.3.1 H_2 column density from CO observations

Cold molecular clouds are primarily traced by the second most abundant molecule, CO, which is asymmetric. The first rotational lines are the most commonly observed transitions at 115, 230 and 345 GHz, with the first lying only ~ 5 K above ground, a relatively low effective density ($\sim 10^{2-3} \text{ cm}^{-3}$) and a wavelength (3 mm) which is readily observable from the ground. It has therefore historically been one of the most commonly used tracers of physical conditions in the molecular ISM. A CO-to- H_2 conversion factor (also called the X factor) can be established based on the 115 GHz line intensity ($T_{mb}(\text{CO})$):

$$N(\text{H}_2) \sim X(\text{CO}) \times T_{mb}(\text{CO}) \quad (1.78)$$

In the galactic molecular clouds $X(\text{CO}) \sim 2 \times 10^{20} \text{ cm}^{-2} (\text{K.km/s})^{-1}$, but this value is dependent on the metallicity [Wilson, 1995, Boselli et al., 2002, Bolatto et al., 2013] with a factor of 2–20 lower towards starburst galaxies [Downes and Solomon, 2003]. The exact value of the conversion factor between CO integrated line intensity and mass, X, is however a matter of some dispute.

An alternative estimate of $N(\text{H}_2)$ using ^{13}CO (or even C^{18}O) emission requires several steps and assumptions. One can assume optically thin ^{13}CO emission or derive the ^{13}CO opacity (τ_{13}), using the T_{mb} (^{12}CO) which is optically thick, as a measure of the ^{13}CO

excitation temperature (see Sec. 1.2.1 and discussion of Fig. 1.4) and then correct the optically thin column density value by the factor $\tau_{13}(V)dV/[1 - \exp(-\tau_{13}(V))]dV$. We can rewrite Eq. 1.26 into:

$$\tau_\nu = -\ln \left[1 - \frac{T_{mb}}{J_\nu(T_{ex}) - J_\nu(T_{CMB})} \right] \quad (1.79)$$

and insert this equation in Eq. 1.50. In the case of optically thin line (cf Eq. 1.28):

$$T_b(v) = [J_\nu(T_{ex}) - J_\nu(T_{CMB})] \times \tau(v). \quad (1.80)$$

Then:

$$N_{tot} = N_{tot}^{thin} \times \frac{\tau}{1 - \exp(-\tau)} \quad (1.81)$$

where the fraction corresponds to the *optical depth correction factor* (see Sec. 1.2.2).

Note that a constant T_{ex} is assumed to estimate the fractional population in all J levels of ^{13}CO . In the low-density regime of molecular clouds, the $J = 1-0$ T_{ex} of ^{13}CO is often smaller than the value determined from ^{12}CO . By adopting the excitation temperature of ^{12}CO , the resultant ^{13}CO column density is therefore underestimated. Finally, to derive the H_2 column density, an isotopic ratio of $^{12}\text{CO}/^{13}\text{CO}$ and $\text{H}_2/^{12}\text{CO}$ abundance ratio are assumed. Based on H_2 and CO IR absorption lines, the H_2/CO abundance ratio ranges from 4,000 to 7,000 [Lacy et al., 1994, Kulesa, 2002]. However, both isotopic and CO abundance ratios can vary within clouds and from cloud to cloud owing to isotopic fractionation and local UV fields. For example, at the center of dense cores, the $[\text{CO}]/[\text{H}_2]$ ratio is expected to be reduced by up to five orders of magnitude [Bergin and Langer, 1997]. This so-called *depletion* is dependent on the temperature, the density and the timescale. Other tools must therefore be used for the determination of H_2 in the cold and dense regions of the ISM.

1.3.2 H_2 column density from dust measurements

Dust grains are made up of metals such as carbon and silicon (with a mass fraction in metals is 1%), so a (more or less) constant gas-to-dust ratio is expected in the ISM. The observations of the dust column density are therefore often used to estimate the total H_2 column density in the gas phase. At millimetric wavelengths, in the Rayleigh-Jeans domain, dust emission depends linearly on temperature, and its great advantage is its optical thinness.

The observed flux density F_ν (Jy beam^{-1}) is approximated with a modified black body curve. For optically thin emission:

$$F_\nu = B_\nu(T_{dust})(1 - e^{-\tau}) = B_\nu(T_{dust}) \times \tau_\nu \quad (1.82)$$

In the (sub)millimetre regime (emission of cold dust), the dust emission is rarely optically thick, except possibly at high resolution or towards high-mass star forming regions. Having F_ν we can deduce τ . The dust opacity is defined as:

$$\tau(\nu) = \rho_{dust} \times \kappa(\nu) \times L \quad (1.83)$$

where ρ_{dust} is the mass density (g cm^{-3}), $\kappa(\nu)$ is the mass absorption coefficient in $\text{cm}^2 \text{g}^{-1}$, L the thickness of structure along the line-of-sight. The so-called dust opacity, $\kappa(\nu)$, which expresses the effective surface area for extinction per unit mass, depends on the chemical composition and structure of dust grains, but not the size for particles. However, κ will be modified in the dense regions of the ISM, with an increase by a factor of 2–3, leading to a higher uncertainty of the mass and abundances determinations [Juvela et al., 2015]. The dust opacity is usually described as a power law $\kappa(\nu) = \kappa_0(\nu/\nu_0)^\beta$ [Hildebrand, 1983, Compiègne et al., 2011], where κ_0 is the emission cross-section at a reference frequency ν_0 . The fit is possible when observations consist of at least three wavelengths covering frequencies before and after the maximum value of the intensity. For example, for cold cores, observations at long wavelengths (beyond 200 μm) are needed to constrain the spectral index, while shorter wavelengths are better for determining colour temperature. For isothermal clouds in the millimeter wavelength range, the spectral index value can be derived using the ratio of the surface brightness at for example 1.2 and 3 mm:

$$\beta = \frac{\log(I_{1.2\text{mm}}/I_{3\text{mm}}) - \log(B_{1.2\text{mm}}(T_{dust})/B_{3\text{mm}}(T_{dust}))}{\log(\nu_{1.2\text{mm}}/\nu_{3\text{mm}})} \quad (1.84)$$

So the fit of the modified blackbody involves three free parameters: the spectral index (β), the colour temperature (T), the intensity (I_0) at a reference frequency ν_0 and B_ν is the Planck function.

We are interested in the H_2 column density:

$$\begin{aligned} N(\text{H}_2) &= \int n_{\text{H}_2} ds = \int \frac{N_b(\text{H}_2)}{\text{Volume}} ds = \int \frac{\text{Mass}}{\text{Volume} \times \mu(\text{H}_2)m_H} ds \\ &= \int \frac{\rho_{gas}}{\mu(\text{H}_2)m_H} ds = \frac{\tau(\nu)}{\mu(\text{H}_2)m_H\kappa(\nu)} \end{aligned} \quad (1.85)$$

where m_H is the hydrogen atom mass, $N_b(\text{H}_2)$ is the number of H_2 molecules, $\mu(\text{H}_2)$ is the total mass (Mass) relative to the H_2 molecule ($N_b(\text{H}_2) \times m_H = N_b(\text{H})/2 \times m_H$ as $N_b(\text{H}) = 2N_b(\text{H}_2)$ in the cold regions of the ISM). As hydrogen represents 71% of the total mass of metals in the ISM we can approximate $\mu(\text{H}_2)$ as 2.8 ($2M(\text{H})/0.71/M(\text{H})$). Note that in the above equation, an assumption on the dust opacity has been made, as the gas-to-dust mass ratio of 0.1 in our Galaxy [Beckwith et al., 1990], has been taken into account:

$$\kappa(\nu) = 0.1(\nu/1000\text{GHz})^\beta, \quad (1.86)$$

assuming a value for the spectral index β (for example, 1.8 is appropriate for dense regions [Juvela et al., 2015]).

In conclusion, when you measure a flux density at frequency ν you can deduce τ from Eq. 1.82. You can now determine the H_2 column density using Eq. 1.85, after computing β (Eq. 1.84) or assuming a value, to determine κ_ν (Eq. 1.86). The beam averaged column density can be expressed as:

$$N(\text{H}_2) = \frac{F(\nu)}{\Omega\mu(\text{H}_2)m_H\kappa(\nu)B_\nu(T_{dust})} \quad (1.87)$$

Ω being the beam solid angle. We can then express the above equation in useful units:

$$N(H_2) = 2.02 \times 10^{20} (cm^{-2}) \left(e^{1.439/[\lambda(mm)(T/10K)]} - 1 \right) (\lambda(mm))^3 \left(\frac{0.1}{\kappa_\nu(cm^2 g^{-1})} \right) \left(\frac{10}{\theta_b('')} \right)^2 (F(\nu)(mJy beam^{-1})) \quad (1.88)$$

1.3.3 Comparison with chemical models

Modellings and simulations of the chemistry, in which the abundances are calculated based on the rates of their formation and destruction, can now be compared to the observations. Since the calculated abundances are function of time as well as the initial conditions of the modelled source, the modelling can provide information about the history of the source. A lot of efforts have been made during the past 10 years to feed the chemical databases based on the astronomical discoveries, but it should be emphasised that models are still imperfects as our knowledge must be improved based on laboratory work and theoretical calculations.

To easily compare the abundances as a function of time, derived from the chemical models, with the observations, we first need to calculate the column density of the modelled molecular species along the radius of the core. We therefore must convert the modelled abundance $[X]$ (with respect to H) of a species X into column densities $N(X)$. The most simple example for a typical prestellar core with a 1D symmetry gives, for a beam smaller than the core:

$$N(X) = 2 \times \sum_{i=2}^n \left(\frac{n(H)_i [X]_i + n(H)_{i-1} [X]_{i-1}}{2} \right) \times (R_{i-1} - R_i) \quad (1.89)$$

where R is the radius from the centre and i the position in the grid along the line of sight ($i = 1$ being the outermost position) composed of n shells. $n(H)_i$ is the gas density at radial point i , $[X]_i$ the abundance of the species. Different column densities are derived depending on the observed position towards the core. The different column densities obtained using Eq. (1.89) must then be convolved with the beam size of the telescope used at the frequency of the observations. The H_2 column density can also be derived using the same method if the density profile of the source is known.

We therefore obtain, from the chemical models, a variation in time of the column density that can be compared with the observed column density to constrain the age using as many species as possible. For that, in order to find the *best-fit* model, we can use the distance of disagreement computation, applied on the column density, which is computed as follows:

$$D(t) = \frac{1}{n_{obs}} \sum_i |\log(N(X))_{obs,i} - \log(N(X))_i(t)| \quad (1.90)$$

where $N(X)_{obs,i}$ is the observed column density, $N(X)_i(t)$ is the modelled column density at a specific age and n_{obs} is the total number of observed species considered in this computation. The distances can be compared with many models with different initial conditions (atomic abundances, temperature, density, etc...) to obtain the lowest value and therefore the *best-fit* age and initial conditions. Fig. 1.6 shows an example of the radial distribution

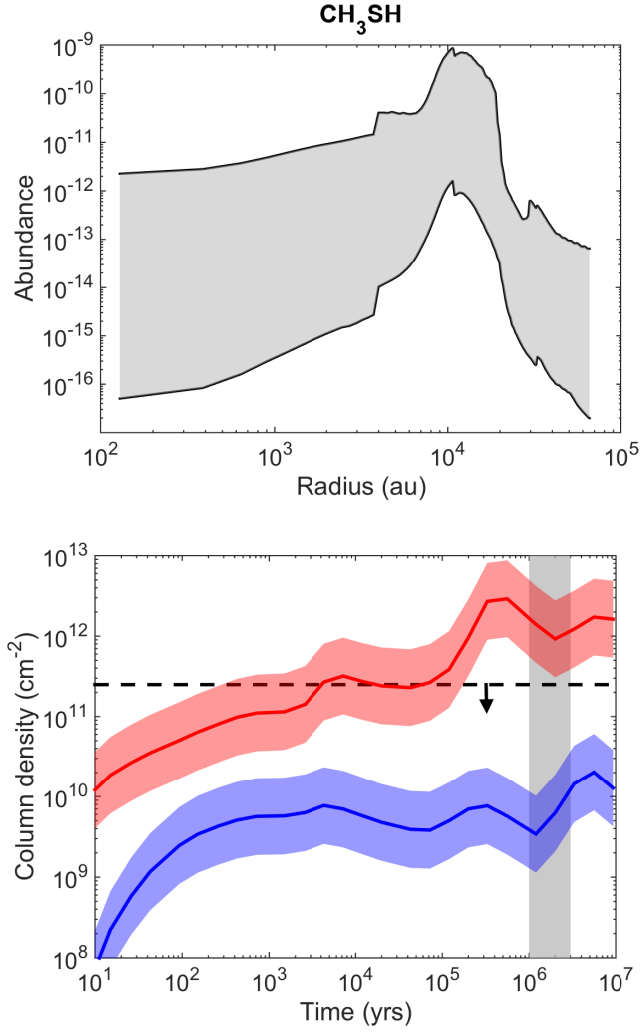


Figure 1.6: Results from a chemical model using the KIDA (<https://kida.astrochem-tools.org/>) database and the NAUTILUS (<https://kida.astrochem-tools.org/codes.html>) chemical code.

of the modelled CH₃SH for an age between 10⁶ et 3 × 10⁶ years already constrained using many species (gray vertical area), for different models (red: non-sulphur depletion and blue: sulphur depletion in the initial atomic abundances) for the prestellar core L1544. The dashed line correspond to the column density computed by Vastel et al. [2018].

Chapter 2

Use of a non-LTE radiative transfer code within CASSIS

2.1 RADEX

You can also use a non-LTE radiative transfer code within the CASSIS software. RADEX is a statistical equilibrium radiative transfer code and is made available for public use as part of the Leiden Atomic and Molecular Database ([LAMDA](#)). It is a one-dimensional non-LTE radiative transfer code, that uses the escape probability formulation assuming an isothermal and homogeneous medium without large-scale velocity fields. RADEX is comparable to the LVG method and provides a useful tool in rapidly analyzing a large set of observational data providing constraints on physical conditions, such as density and kinetic temperature.

If you plan to use RADEX within CASSIS, you have first to download, install and check RADEX :

- Download RADEX from the official [RADEX website](#)
- Install and check RADEX as stated on the RADEX website
- When your RADEX install is working, copy the whole RADEX directory into your current CASSIS directory. This is mandatory because CASSIS will change some files of RADEX, making it unusable outside CASSIS. Do not run RADEX standalone from the RADEX directory in CASSIS, run it from your original install directory. Note that the collisional files in the RADEX/Data directory are not used, as used with RADEX standalone. CASSIS will use the collisional files in its database/lamda directory.

The input parameters are: the kinetic temperature, the density of the collision partner (H_2 , p- H_2 , o- H_2 , electrons, H (atoms), He, and H^+), the molecular column density, the line width and the temperature of background radiation (2.73 K by default). RADEX computes the opacity of the line, the excitation temperature (K), the peak intensity (K) and the line flux (K.km/s) which is simply calculated as the integral of the Gaussian: $\int T_R dv = T_R \times FWHM \times \frac{\sqrt{2\pi}}{2\sqrt{2\ln(2)}}$ where FWHM is the Full Width at Half Maximum

(km/s).

The integrated profile is useful for estimating the total amount of emission in the line, although it has limited meaning for optically thick lines since the changing optical depth over the profile is not taken into account. Using the RADEX code as a standalone version, the entire radiative transfer is performed with rectangular line shapes.

Here is an example of the output from RADEX standalone on the HCO⁺ molecule:

```
* Radex version : 30nov2011
* Geometry : Uniform sphere
* Molecular data file : /Users/vastel/CODES/Radex/data/hco+.dat
* T(kin) [K]: 100.000
* Density of H2 [cm-3]: 1.000E+11
* T(background) [K]: 2.730
* Column density [cm-2]: 3.000E+14
* Line width [km/s]: 1.000
```

Calculation finished in 10 iterations

Line	E_{up}	Freq(GHz)	T_{ex} (K)	τ	T_R (K)	Flux(K.km/s)
2-1	12.8	178.3748	100.0	1.814E+00	7.985E+01	8.500E+01
3-2	25.7	267.5573	100.0	3.670E+00	9.122E+01	9.710E+01
4-3	42.8	356.7338	100.0	5.618E+00	9.132E+01	9.721E+01
5-4	64.2	445.9024	100.0	7.245E+00	8.961E+01	9.539E+01

CASSIS uses the opacity and excitation temperature from the output file, to reconstruct the line profile using equation 1.37 and the equation of a Gaussian line profile. For optically thick lines, CASSIS will broaden the line profile although RADEX keeps a constant FWHM. Linewidths may be different from one line to another due to the opacity effect, therefore one computation for one unique FWHM cannot be done.

For example, Fig. 2.1 shows a synthetic spectrum of the 5-4 transition of HCO⁺ (black line=LTE model with 8 K noise) for the above parameters ($N=3 \times 10^{14} \text{cm}^{-2}$, FWHM=1 km/s, $T_{ex}=100$ K). We perform the RADEX modelling (red line) using a high density so that we reach LTE ($n_{H_2} = 10^{11} \text{cm}^{-3}$), with $T_k = 100$ K. Using a 1km/s line width, the integrated flux intensity from RADEX should be 95.39 K.km/s (see table above), well below the observed flux of ~ 1.8 (km/s) \times 89.6 (K)= 161.3 K.km/s, where 1.8 km/s represents the line width of the observed line (after broadening due to the opacity effect).

Using a 1.8 km/s line width in the standalone RADEX version gives:

Line	E_{up}	Freq(GHz)	T_{ex} (K)	τ	T_R (K)	Flux(K.km/s)
5-4	64.2	445.9024	100.0	4.025E+00	8.807E+01	1.688E+02

with a line flux of 168.8 K.km/s compatible with the modelled flux from CASSIS.

2.2 The collision database

The aim of this database is to provide the community an up-to-date database on the collisional coefficients to be used with the RADEX radiative transfer modelling. These files are mandatory for the non-LTE modelling within CASSIS. To date there are three updated collision databases:

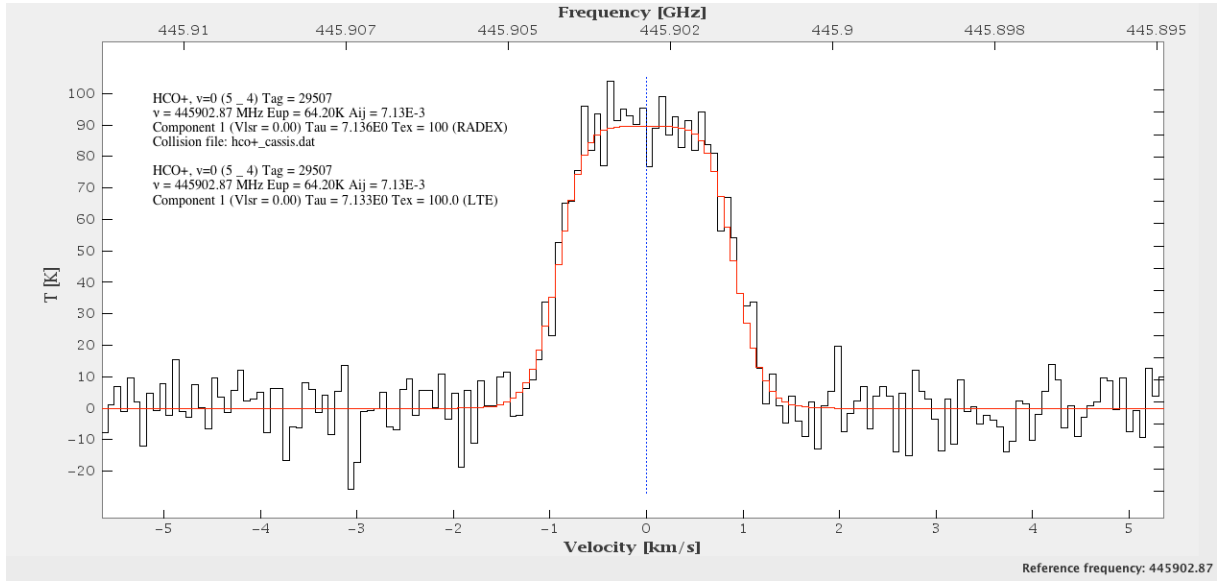


Figure 2.1: Modeled HCO⁺ 5-4 transition in LTE (black) and with RADEX (red) using CASSIS.

- the [LAMDA](#) database maintained by F. van der Tak at the Leiden University (Netherlands),
- the [Basecol](#) database maintained by M.-L. Dubernet at the Paris observatory (France),
- the [EMAA](#) database maintained at IPAG.

The LAMDA and EMMA database has the advantage to provide collision files directly used with the RADEX tool. The Basecol database does not generate files directly used with this tool. RADEX is implemented within the CASSIS software and CASSIS needs to address the quantum numbers associated with the molecular/atomic transitions to perform line identification and generate synthetic spectra for example.

The [collision database provided by CASSIS](#) gathers the most up-to-date collision files provided by LAMDA, BASECOL, and by the scientists feeding the databases (e.g. F. Lique, A. Faure). Those files are made compatible with their associated molecular database (JPL and/or CDMS) so that the quantum numbers, Einstein coefficients, upper energy levels and rest frequencies match. Indeed, some species may have less quantum numbers from database to another and some collision coefficients do merge some K+/-transitions (CH₃CN example). Currently the database contains data for more than 60 molecular species. Several isotopomers and deuterated versions are also available. Work is currently underway to add more data files. We encourage comments from the users in order to improve and extend the database. Here is below the proposed collision files to be used in CASSIS. You can also use your own modified collision rates, but be careful to use the underscore symbol between the quantum numbers.

Example:

```
! LEVEL + ENERGY(CM-1) + WEIGHT + QUANTUM NOS.
```

```
1 0.0000 3.0 0 0 0
```

```
2 2.1346 9.0 1 0 1
```

should be :

```
! LEVEL + ENERGY(CM-1) + WEIGHT + QUANTUM NOS.
```

```
1 0.0000 3.0 0_0_0
```

```
2 2.1346 9.0 1_0_1
```

Then, when using the LTE-RADEX modelling within CASSIS, select your file using Ctrl + left click under the "Collision" tab.

Chapter 3

Molecules (using the JPL or CDMS catalogs) in CASSIS

CASSIS ingests the JPL and CDMS databases as well as their partition functions as a whole in a SQLite database.

3.1 The Einstein A_{ul} coefficients

The line intensity in the catalogs, $I_{ul}(300\text{K})$ is obtained from:

$$I_{ul}(T) = \frac{8\pi^3}{3hc} \nu_{ul} S_{ul} \mu^2 [e^{-E_l/kT} - e^{-E_u/kT}] / Q_{rs}(T) \quad (3.1)$$

where ν_{ul} is the line frequency, S_{ul} is the line strength, μ is the dipole moment along the molecular axis and Q_{rs} is the rotation-spin partition function (using the same zero of energy as E_u and E_l). The units of intensity given in the catalog is $\text{nm}^2.\text{MHz}$

The average spontaneous emission rate from the upper states into the lower states is:

$$A_{ul} = I_{ul}(T) \nu_{ul}^2 \frac{Q_{rs}(T)}{g_u} \frac{1}{e^{-E_l/kT} - e^{-E_u/kT}} \times \frac{8\pi}{c^2} \quad (3.2)$$

where $T = 300 \text{ K}$.

$$A_{ul} = I_{ul}(T) \nu_{ul}^2 \frac{Q_{rs}(T)}{g_u} \frac{1}{e^{-E_l/kT} - e^{-E_u/kT}} \times 2.796410^{-16} \text{ s}^{-1} \quad (3.3)$$

where $I_{ul}(T)$ is in $\text{nm}^2.\text{MHz}$ and ν is in MHz .

3.2 Spin symmetry separation

In the cold regions of the ISM it is important to consider ortho and para (or A and E) states separately. The energy of the lowest rotational or rotation-hyperfine level is 0 by default. The energy of the lowest level for the other spin-modification(s) is usually given

in the documentation. One should consider Q values for the different spin-modifications separately at least at low temperatures. The CDMS database intends to provide this information in the near future.

In the CASSIS database, a catalog (tagged "VASTEL") takes into account the ortho/para/A/E forms for many species such as H₂O, D₂O, H₂S, D₂S, H₂CO, CH₃OH, H₂¹³CO, H₂C¹⁸O, D₂CO, NH₃, NH₂D, CH₃CCH, HCOOCH₃, c-C₃H₂, CH₃CN, H₂D⁺ and D₂H⁺ molecules using either the JPL or CDMS catalogs.

A file called catdir.cat is also provided. Each element of this file has the following format:

TAG: the species tag or molecular identifier (8 or 9 on the 5th digit to separate the ortho/para/A/E symmetry). For example 020091 for o-D₂O, means that the CDMS catalog (original D₂O = 020502) has been used (4th digit) to be compared with 20592 for o-D₂O where the JPL database has been used (original D₂O tag= 020001).

NAME: an ASCII name for the species.

NLINE: the number of lines in the catalog.

QLOG: A seven-element vector containing the base 10 logarithm of the partition function for temperatures of 300 K, 225 K, 150 K, 75 K, 37.5 K, 18.75 K, 9.375 K, respectively. The main interest of having those Q(T_{ex}) for each symmetry, is an accurate computation for the column density for a symmetry state, or in the case of CASSIS, computation of the main beam temperature for a line of a certain symmetry.

VERSION: the version of the calculation for this species in the catalog (starts at number 69).

ALOG: the base 10 logarithm of the partition function for temperature of 300 K as found in the CDMS or JPL database, where the ortho and para forms are not disentangled.

This value is necessary to compute the Einstein coefficients.

Note that the partition functions are provided at temperatures of 300 K, 225 K, 150 K, 75 K, 37.5 K, 18.75 K, 9.375 K. Interpolation is made for temperatures inside this range. So LTE model for lower temperatures (e.g. 6 K) can be problematic. However, CASSIS provides also the computation for lower temperatures than 9.375 K and higher than 300 K for many species. The files are provided in the cassis/database/sqlPartitionMole directory as ascii files. If you plan to make a LTE model outside the usual range [9.375-300] K, you should check whether your species is in this directory. For example, in the case of the para c-C₃H₂ molecule, you can check that the file 38582.txt file in the cassis/database/sqlPartitionMole has a computed partition function as low as 3 K, with a value 2.3 times lower than the value at 9.375 K. By default, CASSIS will use the partition functions provided in this directory. An error message is provided when requesting excitation temperatures outside the range.

example 1: H₂O and D₂O

H₂O and D₂O are asymmetric top molecules, with the dipole moment along the b-axis. They have ortho and para forms. The notation for the transitions is J,K_a,K_c.

For H₂O:

$g_J=3(2J+1)$ Σ K odd : ortho transitions
 $g_J=(2J+1)$ Σ K even : para transitions
 $Q_{para}(T_{ex})=\Sigma g_i e^{-(E_i-E_{0-para})/kT_{ex}}$ where $E_{0-para} = 0$ K
 $Q_{ortho}(T_{ex})=\Sigma g_i e^{-(E_i-E_{0-ortho})/kT_{ex}}$ where $E_{0-ortho} = 34.23$ K
1113342.9640 0.3000 -0.8353 3 0.0000 3 -180031404 1 1 1 0 0 0 0
556936.0020 0.0500 -0.8147 3 23.7944 9 -180031404 1 1 0 0 1 0 1 0

For D₂O:

$g_J=6(2J+1)$ Σ K even : ortho transitions
 $g_J=3(2J+1)$ Σ K odd : para transitions
 $Q_{para}(T_{ex})=\Sigma g_i e^{-(E_i-E_{0-para})/kT_{ex}}$ where $E_{0-para} = 17.43$ K
 $Q_{ortho}(T_{ex})=\Sigma g_i e^{-(E_i-E_{0-ortho})/kT_{ex}}$ where $E_{0-ortho} = 0$ K
607349.6000 0.2000 -1.3353 3 0.0000 18 -20001 303 1 1 1 0 0 0
316799.8100 0.1200 -2.0408 3 12.1170 9 -20001 303 1 1 0 1 0 1

and you can compare with the values provided by CDMS ($Q_{total}(T_{ex})$) with:

$$Q_{total}(T_{ex}) = Q_{ortho}(T_{ex}) + Q_{para}(T_{ex}) \times \exp(-E_{0-para}/T_{ex}) \quad (3.4)$$

Also you can check that it is consistent with the D₂O CDMS database when at the Boltzmann value (2) for $T_{ex} \sim 2$ (see Fig. 3.1). The Boltzmann value is computed as:

$$\frac{o}{p} \text{ratio} = \frac{Q_{ortho}(T_{ex})}{Q_{para}(T_{ex}) \times \exp(-E_{0-para}/T_{ex})} \quad (3.5)$$

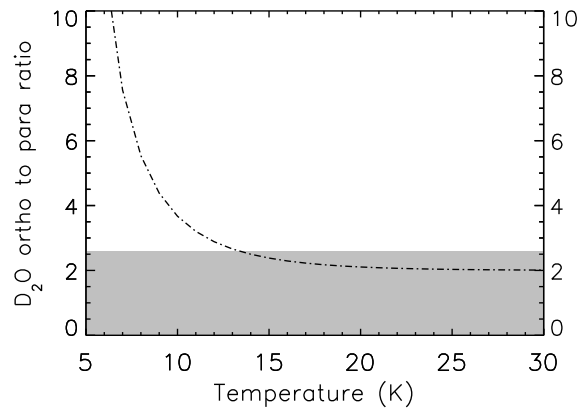


Figure 3.1: The Boltzmann value (dotted-dashed line) for D₂O as a function of temperature. The grey box refers to an upper limit observed with Herschel [Vastel et al. \[2010\]](#)

example 2: H₂S and D₂S

The H₂S and D₂S molecules are asymmetric top molecules. They have ortho and para forms. The notation for the transitions is J,K_a,K_c.

For H₂S:

$$g_J=3(2J+1) \Sigma K \text{ odd : ortho transitions}$$
$$g_J=(2J+1) \Sigma K \text{ even : para transitions}$$
$$Q_{para}(T_{ex})=\Sigma g_i e^{-(E_i-E_{0-para})/kT_{ex}} \text{ where } E_{0-para} = 0 \text{ K}$$
$$Q_{ortho}(T_{ex})=\Sigma g_i e^{-(E_i-E_{0-ortho})/kT_{ex}} \text{ where } E_{0-ortho} = 19.78 \text{ K}$$

452390.3300	0.0700	-2.6154	3	0.0000	3	-34002	303	1	1	1	0	0	0
168762.7624	0.0100	-2.8376	3	13.7463	9	-34002	303	1	1	0	1	0	1

For D₂S:

$$g_J=6(2J+1) \Sigma K \text{ even : ortho transitions}$$
$$g_J=3(2J+1) \Sigma K \text{ odd : para transitions}$$
$$Q_{para}(T_{ex})=\Sigma g_i e^{-(E_i-E_{0-para})/kT_{ex}} \text{ where } E_{0-para}=10.01 \text{ K}$$
$$Q_{ortho}(T_{ex})=\Sigma g_i e^{-(E_i-E_{0-ortho})/kT_{ex}} \text{ where } E_{0-ortho} = 0 \text{ K}$$

91359.1209	0.0230	-4.1358	3	6.9561	9	340	303	1	1	0	1	0	1
237903.6752	0.0581	-3.1702	3	0.0000	18	340	303	1	1	1	0	0	0

example 3: H₂CO and D₂CO

H₂CO and D₂CO are planar asymmetric top molecules but the asymmetry is very small: they are therefore almost prolate symmetric top molecules with the dipole moment along the A-axis. The notation for the transitions is J,K_a,K_c.

For H₂CO:

$$g_J=(2J+1) K_a \text{ is even : para transitions}$$
$$g_J=3(2J+1) K_a \text{ is odd : ortho transitions}$$
$$Q_{para}(T_{ex})=\Sigma g_i e^{-(E_i-E_{0-para})/kT_{ex}} \text{ where } E_{0-para}=0 \text{ K}$$
$$Q_{ortho}(T_{ex})=\Sigma g_i e^{-(E_i-E_{0-ortho})/kT_{ex}} \text{ where } E_{0-ortho} = 15.16 \text{ K}$$

4829.6600	.0010	-5.9024	3	10.5390	9	-30004	303	1	1	0	1	1	1
72837.9480	.0100	-4.1792	3	.0000	3	-30004	303	1	0	1	0	0	0

Then:

$$Q_{tot}(T_{ex}) = Q_{para}(T_{ex}) + e^{-15.16/T_{ex}} Q_{ortho}(T_{ex})$$

For D₂CO:

$g_J=6(2J+1)$ K_a is even : ortho transitions
 $g_J=3(2J+1)$ K_a is odd : para transitions
 $Q_{para}(T_{ex})=\sum g_i e^{-(E_i-E_{0-para})/kT_{ex}}$ where $E_{0-para} = 8.05$ K
 $Q_{ortho}(T_{ex})=\sum g_i e^{-(E_i-E_{0-ortho})/kT_{ex}}$ where $E_{0-ortho} = 0$ K
6096.0673 .0039 -6.2883 3 5.5983 9 32006 303 1 1 0 1 1 1
58468.6700 .1000 -4.1897 3 .0000 18 -32006 303 1 0 1 0 0 0

example 4: H_2D^+ and D_2H^+

These molecules are asymmetric top molecules. The notation for the transitions is J, K_a, K_c .

For D_2H^+ :

$g_I=6(2I+1)$ ΣK even : ortho transitions (warning: different from the documentation file in the CDMS catalog)
 $g_I=3(2I+1)$ ΣK odd : para transitions (warning: different from the documentation file in the CDMS catalog)

The partition function for the ortho transitions will be different than the one for the para transitions. This is necessary in order to estimate the main beam temperature from a column density of a line or to determine the column density from an observation. The need is all the more important as the energy difference between the zero level for the ortho transitions and the zero level for the para transitions is large (see Figure 3.2).

$$Q_{para}(T_{ex})=\sum g_i e^{-(E_i-E_{0-para})/kT_{ex}}$$

$$Q_{ortho}(T_{ex})=\sum g_i e^{-(E_i-E_{0-ortho})/kT_{ex}}$$

where E_{0-para} is the fundamental energy of the para level (50.2 K) and $E_{0-ortho}$ is the fundamental energy of the ortho level (0 K).

$$Q_{para}(T_{ex}=8K)=9.1$$

$$Q_{ortho}(T_{ex}=8K)=6.00$$

$$Q_{para}(T_{ex}=10K)=9.3$$

$$Q_{ortho}(T_{ex}=10K)=6.02$$

$$Q_{para}(T_{ex}=12K)=9.6$$

$$Q_{ortho}(T_{ex}=12K)=6.05$$

$$Q_{para}(T_{ex}=15K)=10.0$$

$$Q_{ortho}(T_{ex}=15K)=6.16$$

For H_2D^+ :

$g_I=3(2I+1)$ K_a odd : ortho transitions

$g_I=1(2I+1)$ K_a even : para transitions

$$Q_{para}(T_{ex})=\sum g_i e^{-(E_i-E_{0-para})/kT_{ex}}$$

$$Q_{ortho}(T_{ex})=\sum g_i e^{-(E_i-E_{0-ortho})/kT_{ex}}$$

where E_{0-para} is the fundamental energy of the para level (0 K) and $E_{0-ortho}$ is the fundamental energy of the ortho level (86.4 K).

$$Q_{para}(T_{ex}=8K)=1.00$$

$$Q_{ortho}(T_{ex}=8K)=9.96$$

$$Q_{para}(T_{ex}=10K)=1.00$$

$$Q_{ortho}(T_{ex}=10K)=10.51$$

$$Q_{para}(T_{ex}=12K)=1.01$$

$$Q_{ortho}(T_{ex}=12K)=11.03$$

$$Q_{para}(T_{ex}=15\text{K})=1.04$$

$$Q_{ortho}(T_{ex}=15\text{K})=11.74$$

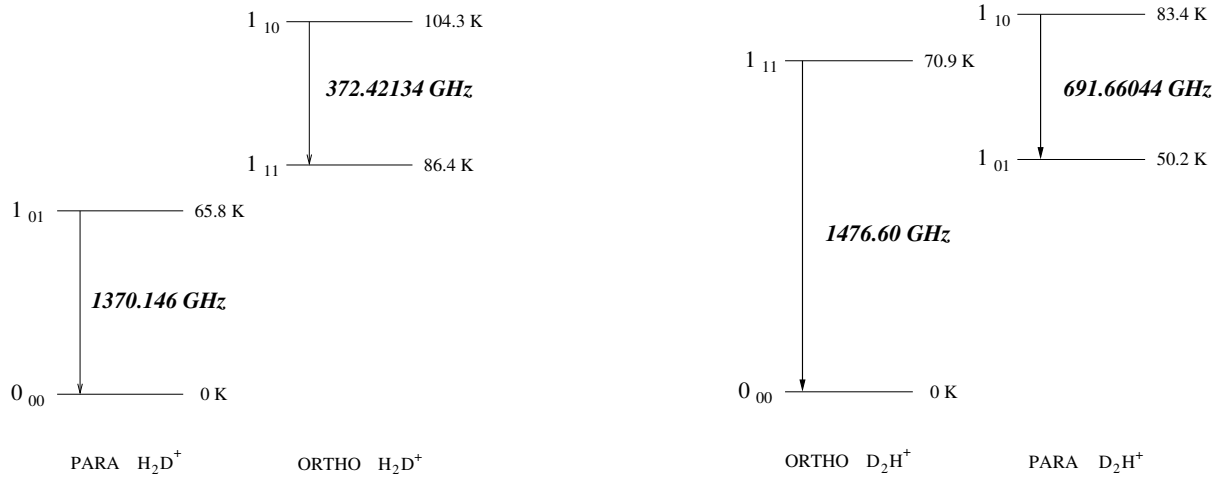


Figure 3.2: Lower energy transitions for the H₂D⁺ and D₂H⁺ molecules.

Bibliography

- S. V. W. Beckwith, A. I. Sargent, R. S. Chini, and R. Guesten. A Survey for Circumstellar Disks around Young Stellar Objects. *AJ*, 99:924, Mar. 1990. doi: 10.1086/115385.
- E. A. Bergin and W. D. Langer. Chemical Evolution in Preprotostellar and Protostellar Cores. *ApJ*, 486(1):316–328, Sept. 1997. doi: 10.1086/304510.
- P. R. Bevington and D. K. Robinson. *Data reduction and error analysis for the physical sciences*. 2003.
- A. D. Bolatto, M. Wolfire, and A. K. Leroy. The CO-to-H₂ Conversion Factor. *ARA&A*, 51(1):207–268, Aug. 2013. doi: 10.1146/annurev-astro-082812-140944.
- A. Boselli, J. Lequeux, and G. Gavazzi. The CO to H₂ Conversion Factor in Normal Late-Type Galaxies. *Ap&SS*, 281(1):127–128, July 2002. doi: 10.1023/A:1019599512232.
- J. I. Castor. Spectral line formation in Wolf-Rayet envelopes. *MNRAS*, 149:111, Jan. 1970. doi: 10.1093/mnras/149.2.111.
- M. Compiègne, L. Verstraete, A. Jones, and et al. The global dust SED: tracing the nature and evolution of dust with DustEM. *A&A*, 525:A103, Jan. 2011. doi: 10.1051/0004-6361/201015292.
- T. M. Dame, D. Hartmann, and P. Thaddeus. The Milky Way in Molecular Clouds: A New Complete CO Survey. *ApJ*, 547(2):792–813, Feb. 2001. doi: 10.1086/318388.
- T. de Jong, S. Chu, and A. Dalgarno. Carbon monoxide in collapsing interstellar clouds. *ApJ*, 199:69–78, July 1975. doi: 10.1086/153665.
- D. Downes and P. M. Solomon. Molecular Gas and Dust at $z=2.6$ in SMM J14011+0252: A Strongly Lensed Ultraluminous Galaxy, Not a Huge Massive Disk. *ApJ*, 582(1):37–48, Jan. 2003. doi: 10.1086/344594.
- M. Elitzur. *Astronomical masers*, volume 170. 1992. doi: 10.1007/978-94-011-2394-5.
- G. A. Fuller and P. C. Myers. Dense Cores in Dark Clouds. VII. Line Width–Size Relations. *ApJ*, 384:523, Jan. 1992. doi: 10.1086/170894.
- P. F. Goldsmith and W. D. Langer. Population Diagram Analysis of Molecular Line Emission. *ApJ*, 517(1):209–225, May 1999. doi: 10.1086/307195.

- P. F. Goldsmith, M. Heyer, G. Narayanan, R. Snell, D. Li, and C. Brunt. Large-Scale Structure of the Molecular Gas in Taurus Revealed by High Linear Dynamic Range Spectral Line Mapping. *ApJ*, 680(1):428–445, June 2008. doi: 10.1086/587166.
- W. Gordy and R. L. Cook. *Microwave Molecular Spectra (New York: Wiley)*. 1984.
- R. H. Hildebrand. The determination of cloud masses and dust characteristics from submillimetre thermal emission. *QJRAS*, 24:267–282, Sept. 1983.
- M. Juvela, I. Ristorcelli, D. J. Marshall, and e. al. Galactic cold cores. V. Dust opacity. *A&A*, 584:A93, Dec. 2015. doi: 10.1051/0004-6361/201423788.
- C. A. Kulesa. *Molecular hydrogen and its ions in dark interstellar clouds and star forming regions*. PhD thesis, University of Arizona, Nov. 2002.
- J. H. Lacy, R. Knacke, T. R. Geballe, and A. T. Tokunaga. Detection of Absorption by H 2 in Molecular Clouds: A Direct Measurement of the H 2:CO Ratio. *ApJ*, 428:L69, June 1994. doi: 10.1086/187395.
- H. S. Liszt and R. Lucas. CO in absorption and emission toward compact extragalactic radio continuum sources. *A&A*, 339:561–574, Nov. 1998.
- J. G. Mangum and Y. L. Shirley. How to Calculate Molecular Column Density. *PASP*, 127(949):266, Mar. 2015. doi: 10.1086/680323.
- D. E. Osterbrock and G. J. Ferland. *Astrophysics of gaseous nebulae and active galactic nuclei*. 2006.
- Y. L. Shirley. The Critical Density and the Effective Excitation Density of Commonly Observed Molecular Dense Gas Tracers. *PASP*, 127(949):299, Mar. 2015. doi: 10.1086/680342.
- V. V. Sobolev. *Moving envelopes of stars*. 1960.
- L. Spitzer. *Physical processes in the interstellar medium*. 1978. doi: 10.1002/9783527617722.
- B. L. Ulich and R. W. Haas. Absolute calibration of millimeter-wavelength spectral lines. *ApJS*, 30:247–258, Mar. 1976. doi: 10.1086/190361.
- E. F. van Dishoeck and J. H. Black. The Photodissociation and Chemistry of Interstellar CO. *ApJ*, 334:771, Nov. 1988. doi: 10.1086/166877.
- C. Vastel, C. Ceccarelli, E. Caux, A. Coutens, J. Cernicharo, S. Bottinelli, K. Demyk, A. Faure, L. Wiesenfeld, Y. Scribano, A. Bacmann, P. Hily-Blant, S. Maret, A. Walters, E. A. Bergin, G. A. Blake, A. Castets, N. Crimier, C. Dominik, P. Encrenaz, M. Gérin, P. Hennebelle, C. Kahane, A. Klotz, G. Melnick, L. Pagani, B. Parise, P. Schilke, V. Wakelam, A. Baudry, T. Bell, M. Benedettini, A. Boogert, S. Cabrit, P. Caselli,

- C. Codella, C. Comito, E. Falgarone, A. Fuente, P. F. Goldsmith, F. Helmich, T. Henning, E. Herbst, T. Jacq, M. Kama, W. Langer, B. Lefloch, D. Lis, S. Lord, A. Lorenzani, D. Neufeld, B. Nisini, S. Pacheco, J. Pearson, T. Phillips, M. Salez, P. Saraceno, K. Schuster, X. Tielens, F. van der Tak, M. H. D. van der Wiel, S. Viti, F. Wyrowski, H. Yorke, P. Cais, J. M. Krieg, M. Olberg, and L. Ravera. Ortho-to-para ratio of interstellar heavy water. *A&A*, 521:L31, Oct. 2010. doi: 10.1051/0004-6361/201015101.
- C. Vastel, D. Quénard, R. Le Gal, and et al. Sulphur chemistry in the L1544 pre-stellar core. *MNRAS*, 478(4):5514–5532, Aug. 2018. doi: 10.1093/mnras/sty1336.
- C. D. Wilson. The Metallicity Dependence of the CO-to-H₂ Conversion Factor from Observations of Local Group Galaxies. *ApJ*, 448:L97, Aug. 1995. doi: 10.1086/309615.